ELSEVIER

Journal of Organometallic Chemistry 552 (1998) 285–292

Journal of Organometallic Chemistry

New chelating silylamido ligands: syntheses and X-ray crystal structures of lithium and magnesium derivatives of [*t*-Bu–HN–$SiMe_2$–*o*-C_6H_4–X] (X = OMe, NMe_2, CH_2NMe_2, CF_3)

Bernd Goldfuss, Paul von Ragué Schleyer *, Sandra Handschuh, Frank Hampel

Institut für Organische Chemie der Universität Erlangen-Nürnberg, Henkestrasse 42, D-91054 Erlangen, Germany

Received 23 July 1997

Abstract

New chelating silylamido ligands with four 'directing metalation donor groups' (DMGs), OMe, NMe_2, CH_2NMe_2 and CF_3 on aryl moieties have been synthesized. The X-ray crystal structures of the dimeric lithium derivatives [{*t*-BuN–$SiMe_2$–*o*-(C_6H_4)–DMG}Li]$_2$ (**1**)$_2$ (OMe), (**2**)$_2$ (NMe_2), (**3**)$_2$ (CH_2NMe_2) and (**4**)$_2$ (CF_3) reveal Li–DMG contacts in all four cases and decreased lone pair-aryl conjugation for OMe and NMe_2. In plane distortions are apparent for the alkyl and silyl substituents of the central (LiN)$_2$ rings in (**1**)$_2$–(**4**)$_2$; these give rise to short 'agostic' Li $\cdots$ H_3C– interactions with the *t*-Bu moieties. While the OMe, NMe_2 and CH_2NMe_2 groups exhibit 'side on' lithium–heteroatom contacts, lithium coordinates to a CF_3 fluorine atom significantly more 'end on'. The ability of the chelating silylamido ligands to coordinate metal ions other than lithium is demonstrated by the X-ray crystal structures of the magnesium complexes [{*t*-BuN–$SiMe_2$–*o*-(C_6H_4)–OMe}$_2$Mg] (**9**) and [{*t*-BuN–$SiMe_2$–*o*-(C_6H_4)–CH_2NMe_2}$(OMe)_2Mg_2$] (**10**). © 1998 Elsevier Science S.A.

Keywords: Lithium; Magnesium; Amides; X-ray crystal analysis; Ab initio computations

1. Introduction

Polar metal amides are widely used in organic and inorganic chemistry, e.g., as non-nucleophilic bases in deprotonation reactions [1–4], hydride transfer reagents [5], synthetic building blocks [6], and as auxiliary ligands [7]. Consequently, molecular [8–13] and electronic structures of lithium organics [11,14] have been investigated extensively [15–18]. An easily variable donor group can be very useful in ligand design, e.g., to modify the strength of metal–ligand interaction [8–13,19].

We have now elucidated the molecular structures of the lithium (**1**–**4**) and some of the magnesium complexes of chelating silylamido ligands with four different, aryl-based 'directed metalation functional groups' (DMGs) [20] as variable donor functions.

First discovered independently by Gilman and Bebb [21] and by Wittig and Fuhrmann [22], DMG's play a crucial role in *ortho*-selectivity due to the acceleration of aromatic metalation reactions [23–25]. While it was first suggested that DMGs influence the ground states of the precursor complexes [26] ('complex-induced proximity effects' [27]), it was demonstrated later that DMGs reduce the activation barriers of the *ortho*-metalations by complexation of the metals in the transition structures ('kinetically-enhanced metallation') [28–33].

2. Syntheses and X-ray crystal structures of [{*t*-BuN–$SiMe_2$–*o*-C_6H_4–X}Li]$_2$ (X = OMe, NMe_2, CH_2NMe_2, CF_3)

The silyl amides **1**–**4** (M = Li) were synthesized by coupling of DMG-functionalized and *ortho*-lithiated benzene derivatives [34,35] with dichlorodimethylsilane and *t*-butyl amine (yielding chelating silyl amines, Scheme 1) as well as subsequent lithiation of the NH functions.

All the lithium amides **1**–**4** (M = Li), which differ only in their DMGs, were crystallized from nonpolar hexane solutions without co-solvent since we wished to

* Corresponding author.

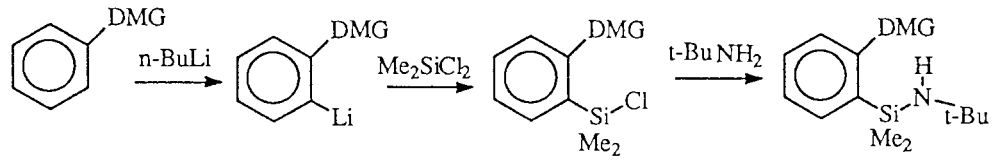

Scheme 1. Synthesis of DMG (OMe, NMe_2, $CH2NMe_2$, CF_3) functionalized chelating silylamines.

Scheme 2. (a) Transition structure of *ortho*-metalation reactions. RM = metalating reagent, e.g., BuLi. (b) Silylamide as model for the DMG coordination in the transition structure of *ortho*-metalation reactions.

elucidate the effects of DMG–lithium coordination in the absence of donor solvent interactions. The chelating silyl amides **1**–**4** are similar to the transition structures of *ortho*-metalation reactions (Scheme 2) [28–33]. Hence, **1**–**4** may serve as models for the individual metal–DMG coordination in the transition structures of *ortho*-metalations [20,23–25,28–35].

The single crystal X-ray analyses reveal dimeric aggregates (Figs. 1–4) with central $(LiN)_2$ rings for all the species $(\mathbf{1})_2$–$(\mathbf{4})_2$ [36].

The Li–DMG interactions are apparent in all four structures $(\mathbf{1})_2$–$(\mathbf{4})_2$: note the short Li–(O, N, F) distances, ranging from 1.95 (O) to 2.19 (F) Å (Table 1). The oxygen atoms in $(\mathbf{1})_2$ exhibit pyramidal environments (Li, Me, C_{aryl} angle sum = 345.6°, Fig. 1). Due to the Li–O coordination, the Me(O) group in $(\mathbf{1})_2$ is not in the plane of the aryl moiety: the Me–O–(C–CH)$_{aryl}$ dihedral angle is 10.2° (Fig. 1) and hence, the

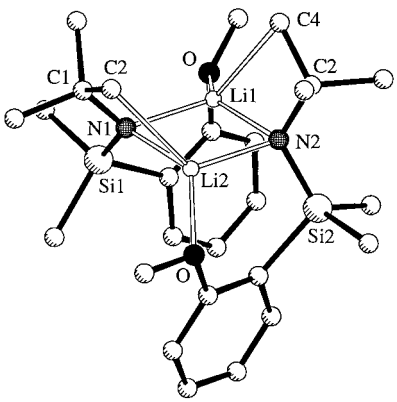

Fig. 1. The X-ray crystal structure of [{*t*-BuN–$SiMe_2$–*o*-(C_6H_4)–OMe}Li]$_2$ $(\mathbf{1})_2$. Hydrogen atoms are omitted for clarity. Distances and angles are given in Tables 1–4.

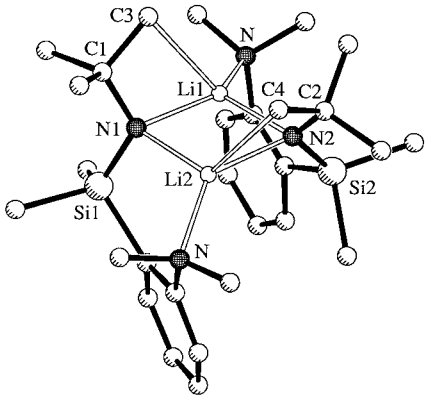

Fig. 2. The X-ray crystal structure of [{*t*-BuN–$SiMe_2$–*o*-(C_6H_4)–NMe_2}Li]$_2$ $(\mathbf{2})_2$. Hydrogen atoms are omitted for clarity. Distances and angles are given in Tables 1–4.

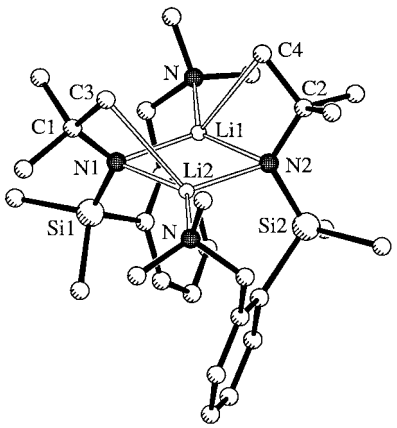

Fig. 3. The X-ray crystal structure of [{*t*-BuN–$SiMe_2$–*o*-(C_6H_4)–CH_2–NMe_2}Li]$_2$ $(\mathbf{3})_2$. Hydrogen atoms are omitted for clarity. Distances and angles are given in Tables 1–4.

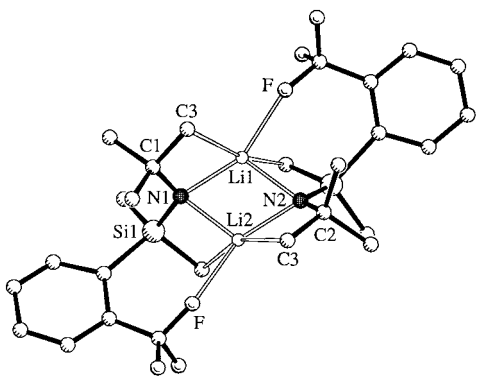

Fig. 4. The X-ray crystal structure of [{*t*-BuN–$SiMe_2$–*o*-(C_6H_4)–CF_3}Li]$_2$ $(\mathbf{4})_2$. Hydrogen atoms are omitted for clarity. Distances and angles are given in Tables 1–4.

Table 1
The lithium–DMG coordination distances (Å) and angles (°) in the X-ray crystal structures $(\mathbf{1})_2$–$(\mathbf{4})_2$ (Scheme 3) and in the computational models **5**–**8** (in parentheses, Scheme 5)

	$(\mathbf{1})_2$ (O atom)	$(\mathbf{2})_2$ (N atom)	$(\mathbf{3})_2^a$ (N atom)	$(\mathbf{4})_2$ (F atom)
Li_1–DMG	1.952(5)	2.050(12)	2.153(9)	2.19(2)
Li_2–DMG	1.958(5)	2.096(13)	2.153(9)	2.28(2)
ϕ(Li–DMG)[b]	1.96 (1.911)	2.07 (2.036)	2.15 (2.037)	2.24 (1.874)
DMG–Li_1–N_1	107.4(2)	112.5((5)	115.5(4)	94.5(7)
DMG–Li_2–N_2	110.6(2)	112.2(6)	115.5(4)	94.1(7)
$\phi(DMG–Li–N)^b_{small}$	109.0	112.3	115.5	94.3
DMG–Li_1–N_2	136.9(3)	134.2(6)	135.2(4)	154.8(10)
DMG–Li_2–N_1	130.2(3)	136.0(7)	135.2(4)	155.4(9)
$\phi(DMG–Li–N)^b_{large}$	133.5	135.1	135.2	155.1
Li_1–DMG–C[c]	102.6(3)	116.2(5)	99.6(4)	150.2(7)
Li_1–DMG–C[c]	105.9(3)	84.5(5)	99.6(4)	149.0(8)
ϕ(Li–DMG–C)[b,c]	104.3 (108.9)	100.4 (102.2)	99.6 (101.1)	149.6 (114.6)

[a] Crystallographic C_2 symmetry.
[b] Average values.
[c] Scheme 4.

O(p-lp)–aryl conjugation is decreased slightly. [1] Structures of lithium aryls with chelating OMe [37,38] and O*t*-Bu [2] functions have been reported.

Lithium coordination prevents effective N(lp)–aryl conjugation in $(\mathbf{2})_2$, even more significantly than in $(\mathbf{1})_2$: the Li–N(Me_2)–(C–CH)$_{aryl}$ torsion angle in $(\mathbf{2})_2$ is 134° and the (Me_2)N–Li axis distorts 46° out of the N–(C–C)$_{aryl}$ plane (Fig. 2) [3]. This competition between lithium coordination and aryl conjugation of the N lone pair was suggested to be responsible for the poor *ortho*-direction quality of the NMe_2 group [24]. The pyramidal NAr(Me_2) environment in $(\mathbf{2})_2$ (average angle sum at N = 329.8°) is clearly apparent (Fig. 3). Structures of 1-lithium aryls with NMe [40,41] groups have been described.

Despite the greater conformational flexibility of the CH_2–NMe_2 group, the N(DMG)–$Li_{(1,2)}$–$N_{(1,2)}$ angles in $(\mathbf{3})_2$ differ not strongly from those in $(\mathbf{1})_2$ and $(\mathbf{2})_2$ (Table 1): small (115.5°) and large (135.2°) DMG–$Li_{(1,2)}$–$N_{(1,2)}$ angles (Scheme 3 left) are clearly apparent in $(\mathbf{3})_2$. The environment of the DMG nitrogen atom in $(\mathbf{3})_2$ is slightly more pyramidal (angle sum = 326.9°) than for N(DMG) in $(\mathbf{2})_2$ (329.8°). X-ray structures of lithium aryls with CH_2NMe_2 [42] groups are known.

As described by Roberts and Curtin [26], the CF_3 group was one of the first DMGs applied in *ortho*-metalations. Although the CF_3 group is suggested to have mostly inductive rather than coordination effects on the metalation reagent in *ortho*-metalation reactions, [24] the $CF_3 \cdots Li$ contact is clearly apparent in $(\mathbf{4})_2$ (Fig. 4). The F–$Li_{(1,2)}$–$N_{(1,2)}$ coordination arrangement of the CF_3 group in $(\mathbf{4})_2$ (Fig. 4) is much more asymmetric

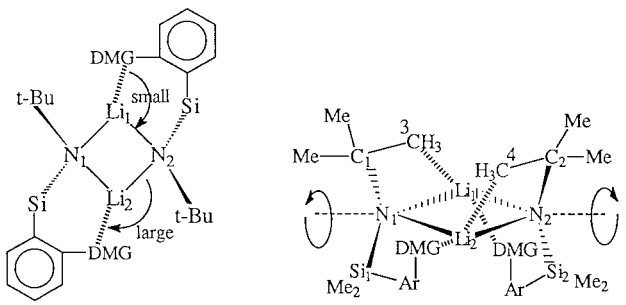

Scheme 3. The structures of $(\mathbf{1})_2$ (DMG = OMe, Fig. 1), $(\mathbf{2})_2$ (DMG = NMe_2, Fig. 2), $(\mathbf{3})_2$ (DMG = CH_2NMe_2, Fig. 3) and $(\mathbf{4})_2$ (DMG = CF_3, Fig. 4). The asymmetric DMG coordinations of lithiums in central $(LiN)_2$ rings (left) and 'in plane' distorsions, resulting in 'agostic' Li $\cdots$ H_3C(*t*-Bu) interactions (right) are shown.

Table 2
The (LiN)2 bond distances (Å) and angles (°) of the X-ray crystal structures $(\mathbf{1})_2$ to $(\mathbf{4})_2$ (Scheme 3 left)

	$(\mathbf{1})_2$	$(\mathbf{2})_2$	$(\mathbf{3})_2^a$	$(\mathbf{4})_2$
Li_1–N_1	1.993(5)	2.064(13)	2.052(9)	1.97(2)
N_1–Li_2	1.993(5)	2.038(12)	2.102(9)	1.98(2)
Li_2–N_2	1.990(5)	2.046(12)	2.052(9)	2.00(2)
N_2–Li_1	2.013(5)	2.003(13)	2.102(9)	1.98(2)
Li_1–N_1–Li_2	70.7(2)	70.3(5)	70.8(4)	70.6(7)
N_1–Li_2–N_2	109.9(2)	108.7(5)	109.2(4)	109.3(8)
Li_2–N_2–Li_1	70.4(2)	71.4(5)	70.8(4)	70.0(7)
N_2–Li_1–N_1	109.0(2)	109.3(6)	109.2(4)	110.1(9)
Li_1–N_1–Li_2–N_2	1.0(2)	4.3(5)	1.3(4)	1.7(8)
N_1–Li_2 N_2–Li_1	−1.0(2)	−4.4(5)	−1.3(4)	−1.7(8)
Li_2–N_2–Li_1–N_1	1.0(2)	4.3(5)	1.3(4)	1.7(8)
N_2–Li_1–N_1–Li_2	−1.0(2)	−4.4(5)	−1.3(4)	−1.7(8)

[a] Crystallographic C_2 symmetry.

[1] For optimal O(lp)-aryl conjugation, the Me–O–(C–CH)$_{aryl}$ angle should be 0°.

[2] See Ref. [39] for the crystal structure of 2,6-di-*t*-butoxyphenyllithium. See Ref. [40] for the crystal structure of 2-dimethylamino-6-*t*-butoxyphenyllithium.

[3] For optimal N(lp)-aryl conjugation, the (Me_2)N–Li axis should be perpendicular to the aryl plane, e.g., Li–N(Me_2)–(C–CH)$_{aryl}$ = 90° (180° − 134° = 46°).

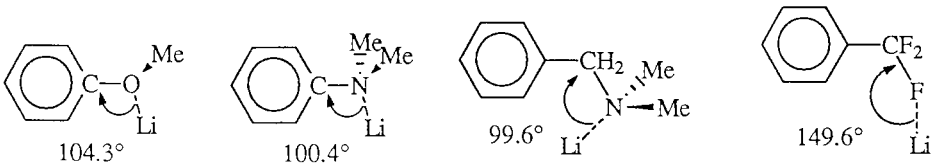

Scheme 4. 'Side on' and 'end on' Li · · · DMG coordinations in the X-ray crystal structures $(\mathbf{1})_2$, $(\mathbf{2})_2$, $(\mathbf{3})_2$ and $(\mathbf{4})_2$ (Table 1).

(smallest 94.3° and largest 155.1° $F–Li_{(1,2)}–N_{(1,2)}$ angles, Table 1) than the $DMG–Li_{(1,2)}–N_{(1,2)}$ coordinations in $(\mathbf{1})_2$, $(\mathbf{2})_2$ and $(\mathbf{3})_2$ (Table 1, Scheme 3 left). This results from the pronounced 'end on' lithium contact to the F–C bond (large $Li_{(1,2)}–F–C$ angle = 149.6°, Table 1), in contrast to the 'side on' Li coordination for DMG = OMe, NMe_2, CH_2NMe_2 (small $Li_{(1,2)}–DMG–C$ angles, Table 1, Scheme 4). While Li · · · F contacts are known for organic $–R_2Si–F$ [43,44] moieties and for inorganic lithium salts, [45] X-ray crystal structures with Li · · · FCF_2 arrangements as in $(\mathbf{4})_2$ have not been reported.

Table 3
Distances (Å) between lithiums $Li_{1,2}$ and the ring (N) substituents $C_{1,2}$ and $Si_{1,2}$ of the X-ray crystal structures $(\mathbf{1})_2$ to $(\mathbf{4})_2$ (Scheme 3 right)

	$(\mathbf{1})_2$	$(\mathbf{2})_2$	$(\mathbf{3})_2^a$	$(\mathbf{4})_2$
$Li_1–C_1$	2.794(5)	2.862(13)	2.884(9)	2.67(2)
$Li_1–Si_1$	3.283(5)	3.242(13)	3.237(9)	3.30(2)
$Li_1–C_2$	3.083(5)	3.235(13)	3.191(9)	3.08(2)
$Li_1–Si_2$	2.859(5)	2.856(13)	2.996(9)	2.76(2)
$Li_2–C_2$	2.796(5)	2.834(13)	2.884(9)	2.679(2)
$Li_2–Si_2$	3.257(5)	3.231(13)	3.237(9)	3.318(2)
$Li_2–C_1$	3.067(5)	3.112(13)	3.191(9)	3.311(2)
$Li_2–Si_1$	2.880(5)	2.917(13)	2.996(9)	2.731(2)
$\phi(Li–C_{short})^b$	2.80	2.85	2.88	2.68
$\phi(Li–C_{long})^b$	3.07	3.12	3.19	3.20
$\phi(Li–Si_{short})^b$	2.87	2.89	3.00	2.75
$\phi(Li–Si_{long})^b$	3.27	3.24	3.24	3.31
$\phi(Li–C)^b$	2.93	2.99	3.04	2.94
$(Li–C)_{deviation}$	0.14	0.14	0.15	0.26
$\phi(Li–Si)^b$	3.07	3.06	3.12	3.03
$(Li–Si)_{deviation}$	0.20	0.18	0.12	0.28

[a] Crystallographic C_2 symmetry.
[b] Average values.

Table 4
Dihedral angles (°) and $Li_{1,2}–C_{3,4}$ 'agostic' distances (Å) in the X-ray crystal structures $(\mathbf{1})_2$ to $(\mathbf{4})_2$ (Scheme 3 right)

	$(\mathbf{1})_2$	$(\mathbf{2})_2$	$(\mathbf{3})_2^a$	$(\mathbf{4})_2$
$Li_1–N_1–C_1–C_3$	3.2(2)	12.1(5)	29.5(4)	11.1(8)
$Li_2–N_2–C_2–C_4$	9.2(2)	11.2(5)	29.5(4)	8.5(8)
$\phi(Li_{1,2}–N_{1,2}–C_{1,2}–C_{3,4})^b$	6.2	11.7	29.5	9.8
$Li_1–C_3$	2.558(6)	2.675(14)	2.788(10)	2.42(2)
$Li_2–C_4$	2.601(6)	2.610(13)	2.788(10)	2.42(2)
$\phi(Li_{1,2}–C_{3,4})^b$	2.58	2.64	2.79	2.42

[a] Crystallographic C_2 symmetry.
[b] Average values.

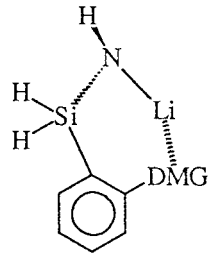

Scheme 5. Computational models for the X-ray crystal structures $(\mathbf{1})_2$ to $(\mathbf{4})_2$: (**5**) (DMG = OMe, Fig. 5); (**6**) (DMG = NMe_2, Fig. 6); (**7**) (DMG = CH_2NMe_2, Fig. 7) and (**8**) (DMG = CF_3, Fig. 8).

The $(LiN)_2$ rings are all nearly symmetrical (similar Li–N distances) and are nearly planar in $(\mathbf{1})_2$ to $(\mathbf{4})_2$ (Table 2). The $(LiN)_2$ ring in $(\mathbf{2})_2$ shows the strongest deviation from planarity (largest Li–N–Li–N torsion angle) among the four structures (Table 2).

As a consequence of the Li–DMG coordination, the alkyl and silyl substituents $C_{(1,2)}$ and $Si_{(1,2)}$ of the $N_{(1,2)}$ central ring atoms bend into the plane of the central $(LiN)_2$ rings slightly; this gives rise to shorter and longer $Li_{(1,2)}–C_{(1,2)}$ and $Li_{(1,2)}–Si_{(1,2)}$ distances (Scheme 3 right, Table 3). The largest deviations from average Li–C and Li–Si distances are apparent for $(\mathbf{4})_2$ (0.26 Å, 0.28 Å, Table 3).

Short 'agostic' [46] Li · · · H_3C contacts (Table 4) of *t*-Bu methyl groups are enabled by the 'in plane' $C_{(1,2)}$ bending (Scheme 3 right, Table 3) as well as favorable *t*-Bu conformations: the $C_{(1,2)}–C_{(3,4)}$ bonds are nearly eclipsed with the $N_{(1,2)}–Li_{(1,2)}$ arrangements. The exception, $(\mathbf{3})_2$, exhibits the largest $Li_{(1,2)}–N_{(1,2)}–C_{(1,2)}–C_{(3,4)}$ torsion angle of 29.5° (Table 4). Only in $(\mathbf{4})_2$, the methyl groups of the $SiMe_2$ moieties increase the lithium

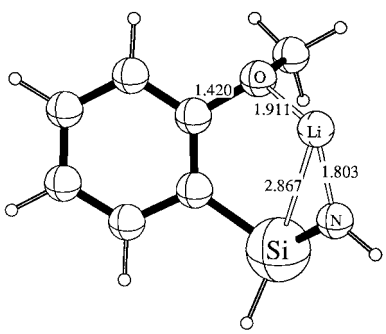

Fig. 5. B3LYP/6-31G* optimized geometry of **5** [*o*-(C_6H_4)–OMe(–NHLi)] (C_1). RHF/6-31G*//RHF/6-31G* frequency computation: NIMAG = 0. Distances in Å.

coordination up to five (Li · · · H_3C(Si) = 2.66(2), 2.71(2), Fig. 4).

3. Computational models

The parent monomeric sub-units (Scheme 5) were computed as theoretical models for the dimeric X-ray crystal structures $(\mathbf{1})_2$ to $(\mathbf{4})_2$ (Figs. 1–4).

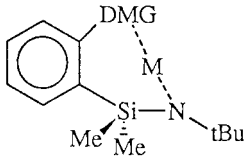

M = Li; DMG = OMe (**1**), NMe_2 (**2**), CH_2-NMe_2 (**3**), CF_3 (**4**)

The B3LYP/6-31G* optimized geometries of **5** to **8** (DMG = OMe, NMe_2, CH_2NMe_2, CF_3) reproduce the DMG–lithium coordination in the corresponding X-ray crystal structures (Figs. 5–8, Table 1). While the 91° distortion of the chelating methoxy group in **5** out of the aryl plane is significantly more than in the experimental

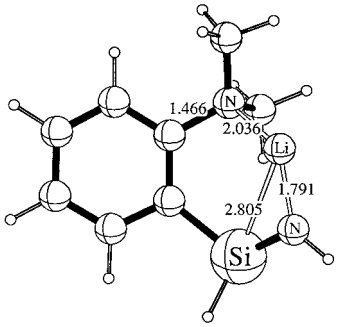

Fig. 6. B3LYP/6-31G* optimized geometry of **6** [*o*-(C_6H_4)–NMe_2(–NHLi)] (C_1). RHF/6-31G*//RHF/6-31G* frequency computation: NIMAG = 0. Distances in Å.

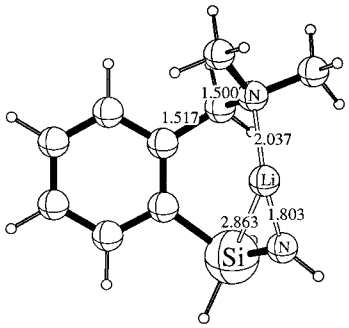

Fig. 7. B3LYP/6-31G* optimized geometry of **7** [*o*-(C_6H_4)–CH_2NMe_2(–NHLi)] (C_1). RHF/6-31G*//RHF/6-31G* frequency computation: NIMAG = 0. Distances in Å.

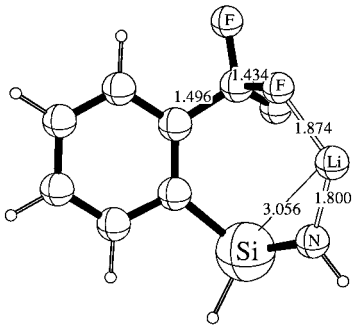

Fig. 8. B3LYP/6-31G* optimized geometry of **8** [*o*-(C_6H_4)–CF_3(–NHLi)] (C_1). RHF/6-31G*//RHF/6-31G* frequency computation: NIMAG = 0. Distances in Å.

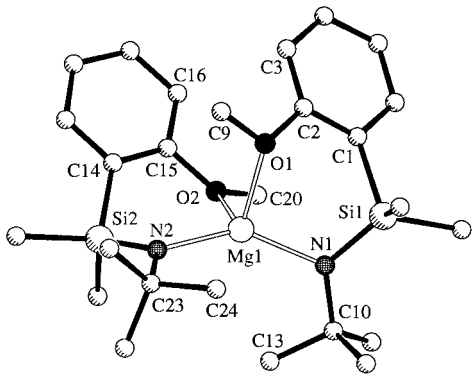

Fig. 9. The X-ray crystal structure of [{*t*-BuN–$SiMe_2$–*o*-(C_6H_4)–Ome}$_2$Mg] (**9**), Table 5. Hydrogen atoms are omitted for clarity.

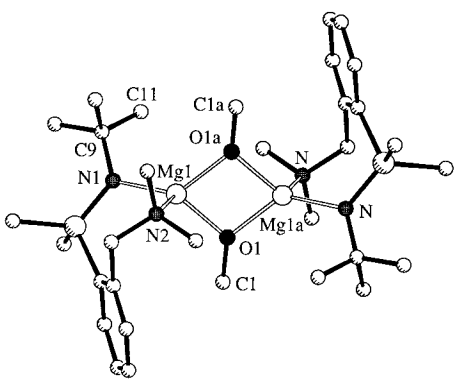

Fig. 10. The X-ray crystal structure of [{*t*-BuN–$SiMe_2$–*o*-(C_6H_4)–CH_2NMe_2}$_2$$(OMe)_2Mg_2$] (**10**), Table 5. Hydrogen atoms are omitted for clarity.

dimer $(\mathbf{1})_2$ (Me–O–(C–CH)$_{aryl}$ = 10°), the Li–N(Me_2) distortion out of the aryl plane is nearly identical in the computed monomer **6** (Li–NMe_2)–(C–CH)$_{aryl}$ = 136°) and in the X-ray crystal structure $(\mathbf{2})_2$ (134°). As in the experimental structure $(\mathbf{4})_2$, the stronger tendency for 'end on' Li–F coordination (large Li–DMG–C angle) of the CF_3 group is reproduced by the computed geome-

Table 5
X-ray crystal data of the magnesium complexes (**9**) (Fig. 9) and (**10**) (Fig. 10)

	(**9**)		(**10**)
O_1–Mg_1	2.084(7)	O_1–Mg_1	1.971(4)
O_2–Mg_1	2.096(6)	O_{1a}–Mg_1	1.971(3)
N_1–Mg_1	1.991(8)	N_1–Mg_1	1.988(4)
N_2–Mg_1	1.995(7)	N_2–Mg_1	2.171(4)
C_{13}–Mg_1	2.981(8)	Mg_1–Mg_{1a}	2.974(3)
C_{24}–Mg_1	3.042(8)	C_{11}–Mg_1	3.237(4)
Mg_1–N_1–C_{10}–C_{13}	6.46°	Mg_1–N_1–C_9–C_{11}	46.89°
Mg_1–N_2–C_{23}–C_{24}	8.34°		

try of **8**; note that **5**–**7** exhibit smaller Li–DMG–C angles (Table 1).

4. X-ray crystal structures of magnesium derivatives

The parent chelating silylamides **1**–**4** (synthesized according to Scheme 2) can be used as ligands for other metalations aside from lithium, e.g., for magnesium. The [{*t*-BuN–$SiMe_2$–*o*-(C_6H_4)–OMe}$_2$Mg] (**9**) and [{*t*-BuN–$SiMe_2$–*o*-(C_6H_4)–CH_2NMe_2}$_2$(OMe)$_2$Mg$_2$] (**10**) complexes provide illustrations (Figs. 9 and 10, Table 5).

Comparisons between **9** and its lithium analogue **1** are instructive. The oxygen atoms in **9** exhibit more planar environments (Mg, Me, C_{aryl} angle sums: 357.9° $O_{(1)}$; 351.8° $O_{(2)}$) than the oxygen atoms in **1** (Li, Me, C_{aryl} angle sum: 345.6°). The bendings of the MeO groups out of the aryl planes are larger in **9** (Me–O–{C–CH}$_{aryl}$: 34.3°, $O_{(1)}$; 23.1°, $O_{(2)}$) than in **1** (10.2°). The conformations of the *t*-Bu groups in **9** result in nearly eclipsed Mg–N–C–Me arrangements (6.5°, 8.3°, Table 5), similarly as in **1** (6.2°, Table 4), and afford Mg · · · Me distances of 2.98 Å and 3.04 Å (Table 5).

Bridging OMe groups in **10** enable a close Mg · · · Mg distance (2.974(3) Å, Table 5, Fig. 10). The degree of pyramidality of the N atoms in the CH_2NMe_2 moieties in **10** (angle sum: 327.0°) is the same as in the CH_2NMe_2 groups in **3** (angle sum: 326.9°). The *t*-Bu conformations in **10** result in staggered Mg–N–C–Me arrangements (46.9°, Table 5) and hence, are even less eclipsed than those in **3** (29.5°, Table 4).

5. Conclusions

Our approach to designing chelating silylamido ligands with readily variable 'directed metalation groups' (DMGs) [20] as donor functions led to the syntheses and X-ray crystal structure analyses of the lithium silylamides **1** to **4** with the DMGs OMe, NMe_2, CH_2NMe_2 and CF_3. All solvent-free dimeric X-ray crystal structures (**1**)$_2$–(**4**)$_2$ exhibit short Li–DMG contacts. The competition of the NMe_2 group between lithium coordination and aryl conjugation is apparent structurally in (**2**)$_2$ and rationalizes the poor *ortho*-selectivity of the NMe_2 group in *ortho*-metalations [24]. The short Li · · · F contact in (**4**)$_2$ emphasizes the ability of the CF_3 group to coordinate centers, first investigated by Roberts and Curtin [26]. While the DMG heteroatoms in OMe, NMe_2, CH_2NMe_2 are coordinated 'side on' by the lithiums, CF_3 prefers 'end on' coordinated fluorine atoms. All structures exhibit short 'agostic' Li · · · H_3C contacts with the *t*-Bu groups and for DMG = CF_3 with H_3C(Si) moieties. As many different DMGs are available [20], this silylamide concept seems attractive for further syntheses of tailor-made ligands [47]. The ability of the ligands [*t*-BuN–$SiMe_2$–*o*-(C_6H_4)–X] (X = OMe, CH_2NMe_2) to chelate other ions than lithium is shown for magnesium in the X-ray crystal structures (**9**) and (**10**).

5.1. Experimental section

The experiments were carried-out under an argon atmosphere by using standard Schlenk as well as needle/septum techniques. The solvents were freshly distilled from sodium/benzophenone. Dichlorodimethylsilane (Me_2SiCl_2), *t*-butyl amine (*t*-$BuNH_2$), anisole (PhOMe), N,N–dimethylaniline ($PhNMe_2$), N,N–dimethylbenzylamine (PhCH2NMe_2) and benzotrifuoride ($PhCF_3$) were purchased from Aldrich. The NMR spectra were recorded on a JEOL GX spectrometer (^{1}H: 400 MHz, ^{13}C: 100.6 MHz) and referenced to TMS. The IR spectra were determined neat between NaCl discs on a Perkin–Elmer 1420 spectrometer and elemental analyses (C, H) on a Heraeus micro automaton. The X-ray crystal data were collected with a Nonius-Mach3 diffractometer using the ω/θ-scan method. The structures were solved by direct methods using SHELXS 86; all data were refined by full matrix least squares on F^2 using SHELXL93 (G.M. Sheldrick, Göttingen 1993). $R1 = \Sigma|F_o - F_c|/\Sigma F_o$ and $wR2 = \Sigma w|(Fo_2 - Fc_2)^2|/\Sigma$ (w $(Fo_2)^2)^{0.5}$. All non-hydrogen atoms were refined anisotropically; the hydrogen atoms were refined independently and isotropically.

5.2. General procedure for the syntheses of aryl dimethylsilyl t-butyl amines (DMG = OMe, NMe_2, CH_2NMe_2, CF_3) as well as their lithium and magnesium derivatives

A solution containing 0.07 mol of the *ortho*-metalated benzene derivative [34] was added slowly at 0°C and under vigorous stirring to a solution of 0.075 mol dichlorodimethylsilane (Me_2SiCl_2, 9.0 g) in 100 ml of diethyl ether. The mixture was stirred 3 h at room temperature and the LiCl precipitate was removed by filtration (glass wool). Diethyl ether and volatile components (e.g., exc. Me_2SiCl_2) were removed by distillation. The residue was taken up in 100 ml of diethyl ether and was slowly added to 1.6 mol *t*-butyl amine (11.8 g) in 100 ml of diethyl ether at 0°C. The mixture

was stirred at room temperature over night (at least 6 h) and the *t*-$BuNH_3Cl$ precipitate was removed by filtration (glass wool). Removal of volatile components (Et_2O, *t*-$BuNH_2$) by distillation and subsequent refined distillation yielded the silylamines. Metalation of the NH functions with *n*-BuLi (1.6 M in hexane) or $MgBu_2$ (1.0 M in heptane) yielded the lithium or magnesium complexes. Traces of methanol led to the OMe incorporation in **10**. Single crystals were grown from cooled hexane or hexane/heptane solutions.

t-BuNH–$SiMe_2$–*o*-(C_6H_4)–OMe, 92% yield, b.p.: 93°C/1 mbar; ^{1}H NMR ($CDCl_3$) δ 7.47 (d), 7.32 (t), 6.93 (t), 6.78 (d), (aryl-*H*), 3.76 (s, O–*CH*$_3$), 1.12 (s, *t*-Bu–*H*), 0.35 (s, Si–*CH*$_3$); ^{13}C{^{1}H} NMR ($CDCl_3$) δ ^{13}C{^{1}H} NMR ($CDCl_3$) δ 164.08, 135.38, 130.56, 128.99, 120.31, 109.55 (aryl-*C*), 54.74 (O–*C*H$_3$), 49.57 (*t*-Bu–*C*), 33.58 (*t*-Bu–*C*H$_3$), 1.57 (Si–*C*H$_3$); IR (neat, cm^{-1}) 3410 (ν N–H), 3080 (ν C_{aryl}-H), 2980–2840 (ν C_{alkyl}-H); IR (neat, cm^{-1}) 3410 (ν N–H), 3080 (ν C_{aryl}-H), 2980–2840 (ν C_{alkyl}-H).

(**1**)$_2$: Anal. ($C_{13}H_{22}Li_1N_1O_1Si_1$) calcd: C: 64.2%, H: 9.1%, found: C: 63.9%, H: 9.2%. X-ray crystal data for (**1**)$_2$: $C_{13}H_{22}Li_1N_1O_1Si_1$, M_r = 243.35; monoclinic; space group P2(1)/n; a = 9.5250(10) Å, b = 18.968(2) Å, c = 16.8660(10) Å, β = 101.670(10)°; V = 2984.2(6) Å3; D_{calc} = 1.083 Mgm^{-3}; Z = 8; F(000) = 1056; Mo–K_α (λ = 0.71073 Å); T = 293 (2) K; crystal size: 0.40 × 0.40 × 0.30 mm; 4° < 2Θ < 48°; reflections collected: 4964, independent: 4655, I > 2σ(I): 3195 data, refined parameters: 308. The final R-values were: $R1$ = 0.0546 (I > 2σ(I)) and $wR2$ = 0.1393 (all data). GOF = 1.078; largest peak (0.203 eÅ^{-3}) and hole (−0.203 eÅ^{-3}).

9: Anal. ($C_{26}H_{44}Mg_1N_2O_2Si_2$) calcd: C: 62.8%, H: 8.9%, found: C: 62.3%, H: 9.1%. X-ray crystal data for **9**: $C_{26}H_{44}Mg_1N_2O_2Si_2$, M_r = 497.12; monoclinic; space group C2/*c*; a = 39.075(7) Å, b = 8.903(5) Å, c = 16.629(7) Å, β = 99.81(2)°; V = 5700(4) Å^3; D_{calc} = 1.159 Mgm^{-3}; Z = 8; F(000) = 2160; Mo–K_α (λ = 0.71073 Å); T = 173 (2) K; crystal size: 0.35 × 0.30 × 0.30 mm; 8° < 2Θ < 52°; reflections collected: 5848, independent: 5761, I > 2σ(I): 1687, refined parameters: 298. The final R-values were: $R1$ = 0.1089 (I > 2σ(I)) and $wR2$ = 0.2503 (all data). GOF = 0.965; largest peak (0.480 eÅ^{-3}) and hole (−0.471 eÅ^{-3}).

t-BuNH–$SiMe_2$–*o*-(C_6H_4)–NMe_2, 82% yield, b.p.: 75°C/1 − 0.5 mbar; ^{1}H NMR ($CDCl_3$) δ 7.68 (d), 7.53 (t), 7.13 (t), 6.98 (d), (aryl-*H*), 2.66 (s, N–C*H*$_3$), 1.17 (s, *t*-Bu–*H*), 0.39 (s, Si–C*H*$_3$); ^{13}C{^{1}H} NMR ($CDCl_3$) δ 160.35, 137.58, 135.61, 129.90, 124.04, 120.58 (aryl-*C*), 49.30 (*t*-Bu–*C*), 46.54 (N–*C*H$_3$), 33.83 (*t*-Bu–*C*H$_3$), 2.85 (Si–*C*H$_3$); IR (neat, cm^{-1}) 3400, 3300 (ν N–H), 3060 (ν C_{aryl}-H), 2980–2780 (ν C_{alkyl}-H).

(**2**)$_2$: Anal. ($C_{14}H_{25}Li_1N_2Si_1$) calcd: C: 65.6%, H: 9.8%, found: C: 64.8%, H: 9.9%. X-ray crystal data for (**2**)$_2$: $C_{14}H_{25}Li_1N_2Si_1$, M_r = 256.39; monoclinic; space group P2(1)/n; a = 10.433(2) Å, b = 15.8158(10) Å, c = 19.198(2) Å, β = 92.26(3)°; V = 3165.5(6) Å^3; D_{calc} = 1.076 Mgm^{-3}; Z = 8; F(000) = 1120; Mo–K_α (λ = 0.71073 Å); T = 293(2) K; crystal size: 0.30 × 0.20 × 0.20 mm; 4° < 2Θ < 48°; reflections collected: 5099, independent: 4940, I > 2σ(I): 2721, refined parameters: 326. The final R-values were: $R1$ = 0.0905 (I > 2σ(I)) and $wR2$ = 0.3138 (all data). GOF = 0.938; largest peak (0.261 eÅ^{-3}) and hole (−0.204 eÅ^{-3}).

t-BuNH–$SiMe_2$–*o*-(C_6H_4)–CH_2NMe_2, 95% yield, b.p.: 87°C/1 − 0.5 mbar; ^{1}H NMR ($CDCl_3$) δ 7.59 (d), 7.38 (d), 7.29 (t), 7.21 (t), (aryl-*H*), 3.61 (s, C*H*$_2$), 2.22 (s, N–C*H*$_3$), 1.14 (s, *t*-Bu–*H*), 0.41 (s, Si–C*H*$_3$); ^{13}C{^{1}H} NMR ($CDCl_3$) δ 144.64, 139.78, 134.83, 129.47, 128.76, 126.10 (aryl-*C*), 64.27 (*C*H$_2$) 49.53 (*t*-Bu–*C*), 45.34 (N–*C*H$_3$), 33.77 (*t*-Bu–*C*H$_3$), 2.97 (Si–*C*H$_3$); IR (neat, cm^{-1}) 3400, 3260 (ν N–H), 3060 (ν C_{aryl}-H), 2980–2720 (ν C_{alkyl}-H).

(**3**)$_2$: Anal. ($C_{30}H_{54}Li_2N_4Si_2$) calcd: C: 66.6%, H: 10.1%, found: C: 65.9%, H: 10.4%. X-ray crystal data for (**3**)$_2$: $C_{30}H_{54}Li_2N_4Si_2$, M_r = 540.83; monoclinic; space group C2/*c*; a = 19.513(3) Å; b = 9.909(2) Å; c = 17.668(2) Å, β = 101.849(11)°; V = 3343.2(8) Å^3; D_{calc} = 1.075 Mgm^{-3}; Z = 4; F(000) = 1184; Mo–K_α (λ = 0.71073 Å); T = 298(2) K; crystal size: 0.30 × 0.30 × 0.30 mm; 6° < 2Θ < 48°; reflections collected: 2700, independent: 2621, I > 2σ(I): 1667, refined parameters: 173. The final R-values were: $R1$ = 0.0837 (I > 2σ(I)) and $wR2$ = 0.2139 (all data). GOF = 1.152; largest peak (0.330 eÅ^{-3}) and hole (−0.320 eÅ^{-3}).

10: Anal. ($C_{16}H_{30}Mg_1N_2O_1Si_1$) calcd: C: 60.3%, H: 9.5%, found: C: 59.8%, H: 10.0%. X-ray crystal data for **10**: $C_{16}H_{30}Mg_1N_2O_1Si_1$, M_r = 318.82; monoclinic; space group P2(1)/n; a = 10.188(2) Å, b = 14.373(3) Å, c = 13.882(3) Å, β = 110.16(3)°; V = 1908.2(7) Å^3; D_{calc} = 1.110 Mgm^{-3}; Z = 4; F(000) = 696; Mo–K_α (λ = 0.71073 Å); T = 223(2) K; crystal size: 0.40 × 0.40 × 0.30 mm; 6° < 2Θ < 48°; reflections collected: 2984, independent: 2984, I > 2σ(I): 1583, refined parameters: 190. The final R-values were: $R1$ = 0.0689 (I > 2σ(I)) and $wR2$ = 0.1868 (all data). GOF = 1.024; largest peak (0.550 eÅ^{-3}) and hole (−0.286 eÅ^{-3}).

t-BuNH–$SiMe_2$–*o*-(C_6H_4)–CF_3, 94% yield, b.p.: 71°C/1.5 mbar; ^{1}H NMR ($CDCl_3$) δ 7.91, 7.65, 7.47, 7.42 (aryl-*H*), 1.12 (s, *t*-Bu–*H*), 0.43 (s, Si–C*H*$_3$); 140.05, 136.54, 135.68, 130.40, 128.72, 120.31 (aryl–*C*), 134.50 (q, *CF*$_3$), 49.65 (*t*-Bu–*C*), 33.44 (*t*-Bu–*C*H$_3$), 1.94 (Si–*C*H$_3$); IR (neat, cm^{-1}) 3600 (ν N–H), 3030 (ν C_{aryl}-H), 2960–2840 (ν C_{alkyl}-H).

(**4**)$_2$: Anal. ($C_{26}H_{38}F_6Li_2N_2Si_2$) calcd: C: 55.5%, H: 6.8%, found: C: 54.8%, H: 7.2%. X-ray crystal data for (**4**)$_2$: $C_{26}H_{38}F_6Li_2N_2Si_2$, M_r = 562.64; triclinic; space group P-1; a = 8.719(2) Å, b = 13.067(3) Å, c = 13.198(3) Å, α = 94.66(3)°, β = 105.58(3)°, γ = 92.15(3)°; V = 1440.8(5) Å^3; D_{calc} = 1.297 Mgm^{-3}; Z = 2; F(000) = 592; Mo–K_α (λ = 0.71073 Å); T =

173(2) K; crystal size: $0.30 \times 0.20 \times 0.20$ mm; $4° < 2\Theta < 50°$; reflections collected: 5096, independent: 5096, $I > 2\sigma(I)$: 2366, refined parameters: 343. The final R-values were: $R1 = 0.1312$ $(I > 2\sigma(I))$ and $wR2 = 0.4598$ (all data). GOF = 0.990; largest peak (1.022 eÅ^{-3}) and hole (-1.161 eÅ^{-3}).

5.3. Computational methods

The theoretical structures were optimized using the gradient techniques implemented in GAUSSIAN 94 [48] with Becke's three parameter hybrid functional incorporating the Lee–Yang–Parr correlation functional (Becke3LYP) [49,50]. The 6-31G* basis set was used. The characters of the stationary points were obtained from analytical RHF/6-31G*//RHF/6-31G* frequency calculations.

Acknowledgements

This work was supported by the Fonds der Chemischen Industrie (also through a scholarship to B.G.), the Stiftung Volkswagenwerk, and the Deutsche Forschungs gemeinschaft.

References

[1] M. Fieser, Reagents for Organic Synthesis, Vol. 15, Wiley, New York, 1990.
[2] B.J. Wakefield, The Chemistry of Organolithium Compounds, Pergamon, Oxford, 1974.
[3] F.E. Romesberg, D.B. Collum, J. Am. Chem. Soc. 117 (1995) 2166.
[4] B.L. Lucht, D.B. Collum, J. Am. Chem. Soc. 117 (1995) 9863.
[5] M. Majewski, J. Organomet. Chem. 470 (1994) 1.
[6] L. Ruwisch, L. Klingebiel, S. Rudolph, R. Herbst-Irmer, M. Noltemeyer, Chem. Ber. 129 (1996) 823.
[7] K. Aoyagi, P.K. Gantzel, K. Kalai, T.D. Tilley, Organometallics 15 (1996) 923.
[8] A.-M. Sapse, P.v.R. Schleyer (Eds.), Lithium Chemistry, Wiley, New York, 1995.
[9] C. Lambert, P.v.R. Schleyer, Angew. Chem. Int. Ed. Engl. 33 (1994) 1129.
[10] C. Lambert, P.v.R. Schleyer, Angew. Chem. 106 (1994) 1187.
[11] C. Lambert, P.v.R. Schleyer, Meth. Org. Chem. (Houben-Weyl), 4th Ed., 1952-, Bd. E19d, 1993, p. 1.
[12] K. Gregory, P.v.R. Schleyer, R. Snaith, Adv. Inorg. Chem. 37 (1991) 47.
[13] R.E. Mulvey, Chem. Soc. Rev. 20 (1991) 167.
[14] M. Veith, S. Müller-Becker, A. Lengert, N. Engel, Oranosilicon Chem., N. Auner, J. Weis (Eds.), VCH, Weinheim, 1994.
[15] B. Goldfuss, P.v.R. Schleyer, F. Hampel, J. Am. Chem. Soc. 118 (1996) 12183.
[16] B. Goldfuss, P.v.R. Schleyer, F. Hampel, J. Am. Chem. Soc. 119 (1997) 1072.
[17] K.G. Caulton, L.G. Hubert-Pfalzgraf, Chem. Rev. 90 (1990) 969.
[18] D.C. Bradley, Chem. Rev. 89 (1989) 1317.
[19] H. Yang, M. Alvarez-Gressier, N. Lugan, R. Mathieu, Organometallics 16 (1997) 1401, and references therein.
[20] V. Snieckus, Chem. Rev. 90 (1990) 879.
[21] H. Gilman, R.L. Bebb, J. Am. Chem. Soc. 61 (1939) 109.
[22] G. Wittig, G. Fuhrmann, Chem. Ber. 73 (1940) 1197.
[23] D.W. Slocum, C.A. Jennings, J. Org. Chem. 41 (1976) 3653.
[24] H.W. Gschwend, H.R. Rodriguez, Org. Reakt. 26 (1979) 1.
[25] N.S. Narasimhan, R.S. Mali, Synthesis (1983) 957.
[26] J.D. Roberts, D.Y. Curtin, J. Am. Chem. Soc. 68 (1946) 1658.
[27] P. Beak, A.I. Meyers, Acc. Chem. Res. 19 (1986) 356.
[28] N.J.R.v.E. Hommes, P.v.R. Schleyer, Angew. Chem. Int. Ed. Engl. 31 (1992) 755.
[29] N.J.R.v.E. Hommes, P.v.R. Schleyer, Angew. Chem. 104 (1992) 768.
[30] N.J.R.v.E. Hommes, P.v.R. Schleyer, Tetrahedron 50 (1994) 5903.
[31] T. Kremer, M. Junge, P.v.R. Schleyer, Organometallics 15 (1996) 3345.
[32] G.A. Suner, P.M. Deyá, J.M. Saá, J. Am. Chem. Soc. 112 (1990) 1467.
[33] J. Morey, A. Acosta, P.M. Deyá, G. Suner, J.M. Saá, J. Org. Chem. 55 (1990) 3902.
[34] L. Brandsma, H. Verkruijsse, Preparative Polar Organometalic Chemistry, Springer, Berlin, 1987.
[35] N.S. Narasimhan, R.S. Mali, Top. Curr. Chem. 138 (1987) 63.
[36] F. Pauer, P.P. Power, Lithium chemistry, in: A.-M. Sapse, P.v.R. Schleyer (Eds.), Wiley, Chichester, 1995, Chap. 9, p. 295.
[37] S. Harder, J. Boersma, L. Brandsma, J.A. Kanters, J. Organomet. Chem. 339 (1988) 7.
[38] S. Harder, J. Boersma, L. Brandsma, G.P.M.v. Mier, J.A. Kanters, J. Organomet. Chem. 364 (1989) 1.
[39] S. Harder, J. Boersma, L. Brandsma, J.A. Kanters, A.J.M. Duisenberg, J.H.v. Lenthe, Organometallics 10 (1991) 1623.
[40] S. Harder, P.F. Ekhart, L. Brandsma, J.A. Kanters, A.J.M. Duisenberg, P.v.R. Schleyer, Organometallics 11 (1992) 2623.
[41] The crystal structure of 2,6-bis(dimethylamino)phenyllithium: S. Harder, J. Boersma, L. Brandsam, J.A. Kanters, W. Bauer, P.v.R. Schleyer, Organometallics, 8 (1989) 1696.
[42] J.T.B.H. Jastrzebski, G.v. Koten, M. Konijn, C.H. Stam, J. Am. Chem. Soc. 104 (1982) 5490.
[43] D. Stalke, N. Keweloh, U. Klingebiel, M. Noltemeyer, G.M. Sheldrick, Z. Naturforsch. 42b (1987) 1237.
[44] D. Stalke, U. Klingebiel, G.M. Sheldrick, J. Organomet. Chem. 344 (1988) 37.
[45] R. Snaith, D.S. Wright, Lithium Chemistry, A.-M. Sapse, P.v.R. Schleyer (Eds.), Wiley, Chichester, 1995, Chap. 8, p. 227.
[46] M. Bookhart, M.L.H. Green, J. Organomet. Chem. 250 (1983) 395.
[47] P. Hofmann, Organometallics in Organic Synthesis, in: A.d. Meijere, H.t. Dieck (Eds.), Springer, Berlin, 1987, p. 1.
[48] Gaussian 94, Revision C.3, M.J. Frisch, G.W. Trucks, H.B. Schlegel, P.M.W. Gill, B.G. Johnson, M.A. Robb, J.R. Cheeseman, T. Keith, G.A. Petersson, J.A. Montgomery, K. Raghavachari, M.A. Al-Laham, V.G. Zakrzewski, J.V. Ortiz, J.B. Foresman, J. Cioslowski, B.B. Stefanov, A. Nanayakkara, M. Challacombe, C.Y. Peng, P.Y. Ayala, W. Chen, M.W. Wong, J.L. Andres, E.S. Replogle, R. Gomperts, R.L. Martin, D.J. Fox, J.S. Binkley, D.J. Defrees, J. Baker, J.P. Stewart, M. Head-Gordon, C. Gonzalez, J.A. Pople, Gaussian, Pittsburgh PA, 1995.
[49] A.D. Becke, J. Chem. Phys. 98 (1993) 5648.
[50] C. Lee, W. Yang, Phys. Rev. B37 (1988) 785.